Template for Submission of Manuscripts to American Chemical Society Journals

Word 2010, Page Wide Abstract Version

This template is a guide to be used to prepare manuscripts for submission. Please consult the Instructions to Authors or a recent issue of the journal for detailed guidelines and procedures for submission. This template is intended to benefit to the author in that the entire manuscript (text, tables, and graphics) may be submitted in one file. Inserting graphics and tables close to the point at which they are discussed in the text of the manuscript can also be a benefit for the reviewer.

When you submit a manuscript using this template, you will not actually see the page formatting that appears in the printed journal. This will occur as part of the editorial production process. Abbreviated instructions for using the template follow. Consult the documentation for your specific application and version for more information. Additional instructions can be found in the readme file at the web page where you downloaded this template.

Using the template

In ACS publications there are many different components of a manuscript (i.e., title, abstract, main text, figure captions, etc.) that are represented in the template. See the Guide, Notes, Notice, or Instructions for Authors on the journal's homepage to determine which parts should be included for the manuscript that you are preparing

1. If typing your manuscript directly into the template, select (highlight) the text of the template that you want to replace and begin typing your manuscript (i.e., select the Title section for typing in your title).
2. If you have already prepared your document in a Word file, you will need to attach the template to your working document in order to apply the Word Style tags. Further instructions can be found in the readme file at the web page where you downloaded this template.
    a. Go to the Word Style list on the formatting toolbar and you will see all the Word Styles from the template that has now been imported into the current document. A Styles toolbar has been generated that will display the different Styles for you to choose from. If this is not present, select **View**, **Toolbars**, and then select **Styles** and it should appear. You can close this at any time and then reopen it when needed.
    b. Click in the sentence or paragraph and then go to the Word Style menu on the toolbar and select the relevant Word Style. This will apply the Word Style to the entire text (sentence or paragraph). Do this for all sections of the manuscript.
3. To insert graphics within the text or as a figure, chart, scheme, or table, create a new line and insert the graphic where desired. If your graphic is not visible, ensure that the Word Style is "Normal" with an automatic height adjustment. If the size of the artwork needs to be adjusted, re-size the artwork in your graphics program and re-paste the artwork into the template (maximum width for single-column artwork, 3.3 in. (8.5 cm); maximum width for double-column artwork, 7 in. (17.8 cm)). **NOTE**: If you are submitting a Table of Contents graphic, please insert the graphic at the end of the file.
4. Ensure that page numbers are present on all pages before submitting your manuscript.
5. Delete these instructions and any sections that are not needed.
6. Save the file with the graphics in place: select **Save As** (**File** menu) and save it as a document file (not a .dot template file).
7. Proof the manuscript to ensure that all parts of the manuscript are present and clearly legible.

Water-soluble nitroxyl porphyrin complexes Fe^{II}TPPSHNO and Fe^{II}TPPSNO$^-$ obtained from isolated Fe^{II}TPPSNO$^\bullet$

Agostina M. Mazzeo, Juan Pellegrino* and Fabio Doctorovich*.

Departamento de Química Inorgánica, Analítica, y Química Física, Facultad de Ciencias Exactas y Naturales, Universidad de Buenos Aires. INQUIMAE-CONICET, Ciudad Universitaria, Pab. 2, C1428EHA, Buenos Aires, Argentina.

KEYWORDS Nitroxyl complexes, porphyrin, water-soluble.

ABSTRACT: The first biomimetic water soluble Fe^{II}-porphyrin nitroxyl complex was obtained, both in protonated and deprotonated forms, and characterized, by reduction of previously isolated and characteized Fe^{II}TPPSNO$^\bullet$. The pKa involved in this equilibrium was estimated to be around 9.7. The Fe^{II}TPPSHNO complex spontaneously reoxidizes to the nitrosyl form following a first order kinetic decay with a measured kinetic constant of k = 0.017 s^{-1}. Experiments show that the HNO adduct undergoes unimolecular homolytic cleavage of the H-NO bond. DFT calculations suggest a phlorin intermediate for this reaction. The deprotonated NO^- complex resulted more stable, with a half-life of about 10 minutes.

Introduction

Nitric oxide (NO$^\bullet$) and nitroxyl (HNO/NO^-) have been consistently studied during recent years due to their biological as well as chemical relevance. Previously only regarded as an environmental pollutant, nitric oxide's role as a signaling agent in living organisms has already been established, acting in vasodilation and nerve signal transduction at low concentrations.[1,2] Recent investigations have also suggested that endogenous generation of the reduced nitroxyl species is possible at physiological conditions,[3–5] which implies that HNO/NO^- could have independent signaling activity of its own, and might also be responsible for some of the physiological effects initially attributed to NO$^\bullet$, like protection against ischemia related injuries.[6–8] Heme proteins are one of the principal targets for these molecules in biological systems, as they tend to bind to metal centers through the nitrogen atom.[9]

In addition, such heme-protein adducts of metal-site coordinated NO$^\bullet$/HNO/NO^- species are key intermediates in the mechanism of action of different enzymes of the nitrogen biogeochemical cycle, such as nitrite or nitric oxide reductases.[10–12] These considerations make it vital to develop biomimetic models of such active sites in order to study their reactivity and structure. Thus, nitrosyl/nitroxyl porphyrin iron complexes have become particularly interesting to study from a bioinorganic point of view.

The increasing number of reports on {FeNO}^{8} (according to the Enermark-Feltham notation)[13] complexes have contributed to the spectroscopic characterization of this initially elusive species but still much more investigation is needed to elucidate mechanistic issues.[14] The first porphyrinate iron-nitroxyl complexes were reported by Kadish et al., using TPP (meso-tetraphenylporphyrin) and OEP (β-octaethyl-meso-tetraphenylporphyrin), by one-electron UV electrochemical reductions of the nitrosyl {FeNO}^{7} analogues, in dichloromethane.[15,16] Later on, both complexes could be obtained chemically and electrochemically by Ryan's group, and further stabilized in THF solution, which allowed their characterization by FT-IR spectroscopy.[17,18] Evidence for the protonated [(OEP)Fe(HNO)] complex was also obtained, resulting stable for hours organic media in the presence of phenols as proton sources.[19] The hexacoordinated derivative [(OEP)Fe(HNO)(5-MeIm)] was prepared via hydride attack on the corresponding ferric nitrosyl by Richter-Addo et al. and characterized by ^{1}H NMR, although in 11% yield and at -20°C.[20] A particularly stable {FeNO}^{8} complex reported by our group could be isolated and characterized by UV-Vis, IR and ^{15}N NMR, using the perhalogenated porphyrin $TFPPBr_8$, in organic media.[21] Nevertheless, attempts to protonate the species to give the expected {Fe**H**NO}^{8} complex were unsuccessful, reacting to give the {FeNO}^{7} complex (Fe^{II}NO$^\bullet$). Lehnert et al. observed analogue results with other electron-poor porphyrins, and more interestingly, reported the first ferrous-heme HNO complex using a very sterically hindered *picket fence* porphyrin, supporting a bimolecular reoxidation pathway hypothesis for unhindered porphyrins in organic media.[22] This complex resulted of great stability, decomposing completely only after ~ 20 h.

Regarding aqueous chemistry the only examples reported consist of the nitroxyl-myoglobin adduct, Mb-HNO,[23] and other analogue globin adducts[24] studied by Farmer and coworkers. The myoglobin-HNO adduct could even be characterized by Raman, NMR and X-ray absorption.[25] These complexes evidence that the protein's distal pocket residues could stabilize the HNO moiety by hydrogen bonding. No biomimetic water-soluble iron heme complex has been stabilized or characterized in aqueous solution.

On the other hand, a very stable water-soluble (although non-heme) {FeNO}^{8} complex could be obtained upon two-electron reduction of $[Fe(CN)_5(NO)]^{2-}$ and characterized spectroscopically, in both its protonated and non-protonated form.[26] The pKa for $[Fe(CN)_5(HNO)]^{3-}$ was estimated via ^{1}H NMR to be about 7.7, giving the first experimental value for bound HNO. The special stability reported for this complex led us to consider that other factors, like hydrogen bonds, could stabilize the Fe-HNO moiety.

In this work we isolated for the first time the {FeNO}^{7} adduct of the water-soluble porphyrin TPPS (meso-tetra(4-sulfonatophenyl)porphine), which has been widely used in previous works on NO chemistry (Figure 1).[27,28] Moreover, we chemically obtained the corresponding {FeNO}^{8} elusive adducts, Fe^{II}TPPSHNO and Fe^{II}TPPSNO$^-$, making these complexes the first ferrous-heme water-soluble nitroxyl models. The products have been characterized by UV-Vis, and cyclic voltammetry experiments. The pKa for Fe^{II}TPPSHNO deprotonation was estimated using spectrophotometric and electrochemical methods. The spontaneous reoxidation reaction of the protonated form to the {FeNO}^{7} adduct Fe^{II}TPPSNO• was kinetically studied via experimental measurements and DFT calculations.

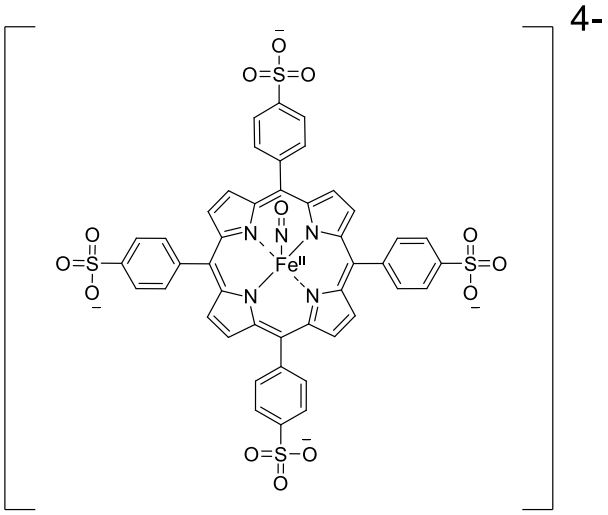

Figure 1. Fe^{II}TPPSNO• anionic moiety. Sodium counterions were omitted for clarity.

Experimental Section

Equipment and measurements

All UV-vis measurements were carried out using a Hewlett-Packard HP8453 diode array spectrometer with 1 cm or 0.2 cm pathlength cuvettes. All NMR measurements were carried out in a BRUKER AVANCE NEO 500 MHz spectrometer. All IR measurements were made using a Thermo Nicolet Avatar FT-IR spectrophotometer. Elemental analysis was carried out in a Carlo Erba EA 1108 system for C, N and H by INQUIMAE. The sample was fully combusted. CO_2, H_2O and N_2 generated were separated by gas chromatography and quantified after thermal conductivity detection. Cyclic voltammetry experiments were carried out using a Princeton Applied Research (PAR) 273A instrument and a PAR303A mercury drop electrode (area 0.024 cm^2), a Ag/AgCl reference electrode (3.0 M KCl), and a platinum wire counter electrode.

Materials

Meso-tetra(4-sulfonatophenyl)porphine in the form of the tetrasodium, dodecahydrate salt ($Na_4TPPS•12H_2O$) was purchased from Frontier Scientific and used as received.

Buffers were freshly prepared with recently degassed water before every experiment. Sodium phosphate monobasic and dibasic salts were purchased from Carlo Erba. Citric acid, sodium carbonate and sodium tetraborate salts were purchased from Biopack. Sodium hydroxide was purchased from Dorwil.

Sodium dithionite (82%) was purchased from Sigma Aldrich and recrystallized following literature procedures[29] in order to increase its purity and separate unwanted disproportion byproducts. This reagent was stored always in a freezer under argon. Solutions of this compound were always made basic (pH $\geq$ 10) in order to minimize decomposition reactions.

Gaseous NO was produced anaerobically from a mixture of $NaNO_2$, NaBr, $FeSO_4$ (Biopack) and 5 ml purged mQ water according to literature techniques.[30]

2,2,6,6-Tetramethylpiperidine 1-oxyl, (TEMPO) was purchased from Sigma Aldrich and used as received for qualitative experiments.

Tetrafluoro boric acid 48% wt. water solution was purchased from Sigma Aldrich, and was deoxygenated by argon bubbling before use.

DFT calculations

All calculations were carried out with the program package Gaussian 09. Meso-tetraphenyl porphyrin (TPP) was used as a model. The structures of all molecules were fully geometry optimized at the DFT level, using the PBE exchange-correlation functional. LANDL2DZ basis set and pseudopotential were used for the Fe atom. For the remaining atoms (H, N, O, C) the 6-31G** basis set was used. Energy scans were performed, and the QST3 method was used as implemented to optimize the geometry of the transition state.

Anoxic atmosphere considerations

All experiments involving Fe^{II}TPPSNO• were carried out under strict anaerobic conditions. A Schlenk argon-vacuum line and appropriate Schlenk glassware were used throughout the development of this work. When necessary, air-sensitive compounds were manipulated inside a nitrogen glove

box. All solids were purged with various argon-vacuum cycles, and liquid reagents and solvents were deoxygenated using techniques varying from argon bubbling (acid solutions) to freeze-pump-thaw (organic solvents, except methanol) or direct vacuum methods (water and methanol). Quartz cuvettes of 1 cm and 2 mm pathlengths topped with new septa were used each time to avoid oxygen filtration. Gastight Hamilton syringes ranging from 10 µL to 5 mL were used for the correct manipulation of the air-sensitive solutions and gases.

Preparation and isolation of $Fe^{II}TPPSNO^{\bullet}\cdot Na_4$ (**1**)

$Na_4TPPS\bullet 12H_2O$ was metallated according to literature techniques,[31] but replacing the tenfold excess of $FeSO_4$ salt with much smaller amounts of $FeCl_2$. This gave chloride salts as byproducts, which resulted much easier to wash than their sulphate analogues. Approximately 200 mg (0.16 mmol) of free porphyrin were mixed with 1.5 equivalents of $FeCl_2$ and 2 eq. NaOH. The reaction was carried out in a water reflux, under argon flow, in order to avoid early oxidation of the ferrous reactant. The process was monitored by UV-vis spectroscopy until full conversion was achieved. Extra base or $FeCl_2$ were added when necessary. The resulting solution was passed through a DOWEX cation exchange column to remove excess Fe^{3+} ions and afterwards alkalinized to pH = 5. The solvent was pumped out and the resulting solid was repeatedly recrystallized by adding distilled acetone to a saturated aqueous solution of the compound until no more traces of chloride (checked by AgCl formation after addition of $AgNO_3$) were found in the supernatant. The product, iron meso-tetra(4-sulfonatophenyl)porphine ($Fe^{III}TPPS$) was dried under vacuum and stored at room temperature. Yield: 124 mg, 62 %.

The five coordinated nitrosyl ferrous complex ($Fe^{II}TPPSNO^{\bullet}$) was obtained by reaction of the ferric porphyrinate with an HNO donor, as reported in literature for porphyrin nitrosyls in organic media.[32] Approximately 40 mg of $Fe^{III}TPPS$ were dissolved in 0.5 ml water along with 1.5 equivalents of 4-fluoro-N-hydroxybenzenesulfonamide (fluoro-Piloty's Acid, fluoro-PA, Figure S1) in the presence of two equivalents of NaOH (See Results, Scheme 1). Fluoro-PA was synthesized according to literature methods[33] and further purified using a silica gel chromatography column as reported independently.[34] The identity and purity of the resulting compound was monitored by ^1H in d^6-DMSO (Sigma Aldrich). The nitrosylation reaction was carried out in water at room temperature, under argon atmosphere and constant stirring. A different Piloty's acid derivative, nitro-PA (synthesized analogously) also proved useful for this reaction, and other variants may be tried, as long as they are at least partially water soluble. Conversion was followed by monitoring the Soret bands corresponding to the reactant and the product in the UV-vis region (395 and 414 nm respectively). Additional base and Piloty's acid equivalents were added when needed. The product was precipitated by addition of degassed acetone. The remaining solid was recrystallized twice analogously (H_2O/acetone) and washed with acetone until Piloty's acid subproducts were no longer detectable by spectrophotometry in the UV region. The resulting red solid, $Fe^{II}TPPSNO^{\bullet}\cdot Na_4$, **1**, was stored under argon in a Schlenk tube. This product, although very air-sensitive when in solution, proved to be quite stable as a solid, and was characterized by IR in Fluorolube and elemental analysis. N-O stretching was observed at 1668 cm^{-1} (Figure S2). This value is in good agreement with literature data of iron nitrosyl porphyrin compounds.[6] Elemental analysis: **Anal. Calc. for $Fe^{II}TPPSNO\bullet Na_4 \bullet 5(H_2O) \bullet 3(CH_3COCH_3)$: %C** 46.8 **%N** 5.1 **%H** 3.8 **Exp: %C** 46.4 **%N** 5.1 **%H** 3.7 A 3/1 acetone/porphyrin mole proportion was verified by ^1H NMR spectroscopy in d^4-MeOH (Figure S3, Table S1). It is soluble in water and, to a lesser extent, in methanol; it is insoluble in other organic solvents. λmax = 414 nm, ε = 155000 M^{-1} cm^{-1}

Kinetic measurements

Experiments to determine the kinetic parameters of the reoxidation reaction were carried out in the UV-vis range using a 2 mm pathlength quartz cuvette. Absorbance traces at 414 and 418 nm (**1** and **2** Soret band peak wavelength respectively) were monitored. Kinetic measurements were made after 1.5-2 eq. of dithionite were added to a solution of **1**. Cycle time was set to 1 s and the experiments ran for about 5 minutes. These experiments were carried out in a variety of conditions, of which the most studied was in 2 mM phosphate buffer at pH = 6. They were also carried out in phosphate at pH = 7 and citrate buffers at pH = 5 of the same concentration and in plain distilled and degassed water, using in this case a non-buffered, pH neutral dithionite solution prepared immediately before use.

The kinetic data were analyzed making a deconvolution of the total absorbance registered at 418 nm. Considering that initially the only species present is **1**, whose absorption spectra and molar absorptivity were already reported,[35] and having calculated the molar absorptivity coefficient of **2** (See Results section), the molar fraction of the nitroxyl compound and its absorbance was calculated as a function of time. Integral kinetic method's plots and fitting were made in order to determine whether the decay followed an order 0, 1 or 2 behavior. Afterwards, appropriate fittings were made with Origin Pro 8 to estimate the associated rate constant. Multiwavelength analyses were also performed using MatLab and proved to give according results.

Results and Discussion

Preparation and isolation of $Fe^{II}TPPSNO^{\bullet}\cdot Na_4$

The product was successfully prepared and isolated as a aolid as shown in the reactions shown in Scheme 1, following reaction path A using an HNO donor, or reaction path B, involving reduction followed by NO gas bubbling. In order to isolate relatively large amounts of compound (20-30 mg), path A was chosen over path B, since the HNO donor byproduct is easily washed off the product by acetone, unlike dithionite byproducts. However, path B, either

for *in situ* or isolation purposes resulted useful for UV experiments and particular bulk experiments. Other reducing agents such as $Cr^{II}EDTA$ and BH_4^- also proved useful for reduction of $Fe^{III}TPPS$.

Scheme 1. Preparation and isolation of $Fe^{II}TPPSNO^{\bullet}\cdot Na_4$. Sodium counterions were omitted for clarity.

A)

$Fe^{III}TPPS^{3-}(aq) + R\text{-}Ph\text{-}SO_2NHOH\ (aq) \longrightarrow$

$\longrightarrow Fe^{II}TPPSNO^{\bullet\,4-}(aq) + R\text{-}Ph\text{-}SO_2H\ (aq)$

B)

1) $Fe^{III}TPPS^{3-}\ (aq) + S_2O_4^{2-}\ (aq) \longrightarrow Fe^{II}TPPS^{4-}\ (aq) + prod\ (aq)$ 2) $Fe^{II}TPPS^{4-}\ (aq) + NO(g) \longrightarrow Fe^{II}TPPSNO^{\bullet\,4-}\ (aq)$

$Fe^{II}TPPSNO^{\bullet\,4-}\ (aq) \xrightarrow{acetone} Fe^{II}TPPSNO^{\bullet\,4-}\ (s)$

Once precipitated by acetone addition, the product was vacuum-dried and stored in a Schlenk tube under argon. This allowed us to manipulate the nitrosyl compound in a relatively simple manner by directly weighing the solid inside the glovebox before the experiments. Furthermore, it allowed us to characterize the compound through IR and elemental analysis techniques for the first time, and carry out cyclic voltammetry and UV-vis experiments using solid **1** as the starting material instead of having to generate the species in situ through chemically unclean paths.

UV scale experiments - Obtention and characterization of $Fe^{II}TPPSHNO^{4-}$ (**2**) and $Fe^{II}TPPSNO^{5-}$ (**3**) in aqueous media

A deoxygenized solution (approx. 5-6 μM) of $Fe^{III}TPPS$ in 2 mM phosphate buffer solution at pH = 6 was treated with 1.5-2 equivalents of sodium dithionite to give $Fe^{II}TPPS$. Excess NO (g) was then added to the mixture to produce **1**, and finally 1-2 more equivalents of dithionite were added to give the desired product, **2** (Scheme 2). The observed spectrum peak of the Soret band shifted from 414 to 418 nm and the corresponding molar absorption coefficient increased from 1.55 10^5 to 2.17 10^5 $M^{-1}\,cm^{-1}$ (Figure 2). Although this product rapidly reoxidized to **1**, in presence of excess dithionite and NO (g) a steady-state regime was reached, allowing us to determine its molar absorptivity coefficient. Seki et al.[35] transiently obtained the same UV spectrum through flash photolysis techniques using benzophenone ketyl radicals and reported the adduct's instability, with a half-life time of 2 seconds. Note that here, we established that under these conditions, the adduct exists in the protonated form, $Fe^{II}TPPSHNO$ (**2**), and not as $Fe^{II}TPPSNO^{-}$ (**3**): see further experiments below.

Scheme 2. Indirect formation and subsequent reoxidation of $Fe^{II}TPPSHNO$ in phosphate buffer at pH = 6.

$Fe^{III}TPPS \xrightarrow{Na_2S_2O_4} Fe^{II}TPPS$

$Fe^{II}TPPS \xrightarrow{NO\ (g),exc.} Fe^{II}TPPSNO^{\bullet}$

$Fe^{II}TPPSNO^{\bullet} \underset{reoxidation}{\overset{Na_2S_2O_4,\ pH=6}{\rightleftharpoons}} Fe^{II}TPPSHNO$

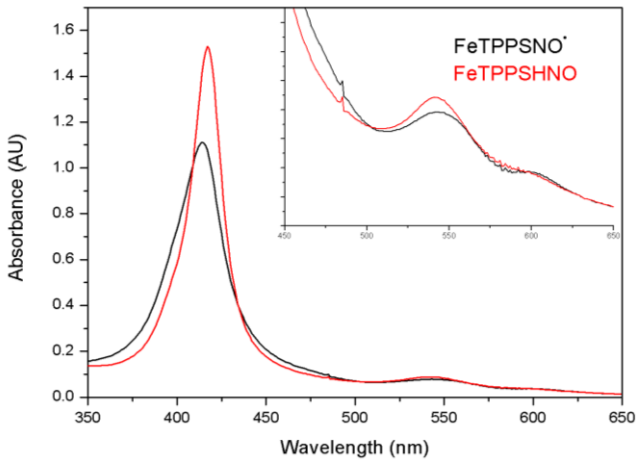

Figure 2. UV-Vis Spectral changes observed upon reduction of $Fe^{II}TPPSNO^{\bullet}$ at pH = 6.

The same was observed when 1-2 equivalents of dithionite were added directly to a freshly prepared 5-6 μM solution of $Fe^{II}TPPSNO^{\bullet}$, in a more controlled, clean manner. In both cases, the resulting **2** complex spontaneously reoxidizes to the $\{FeNO\}^7$ nitrosyl compound, **1** (Figure 3).

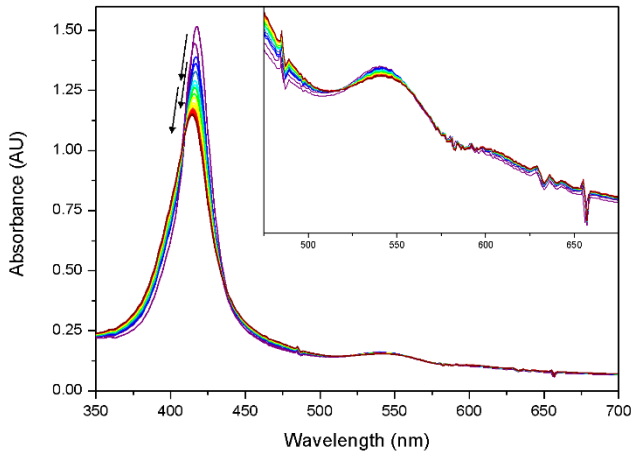

Figure 3. Observed reoxidation of $Fe^{II}TPPSHNO$ to $Fe^{II}TPPSNO^{\bullet}$ at pH = 6. The time elapsed between the maximum and minimum peak is ca. 200 s.

The same experiments were carried out at pH = 12 phosphate buffer, and in this case a different spectrum emerged for the $\{FeNO\}^8$ adduct, which we tentatively assigned to the deprotonated complex, $Fe^{II}TPPSNO^{-}$ (**3**). In this case, a subtle decrease in absorbance was observed for the Soret band, at 413 nm, as well as a slight widening of the band. The most important change was observed in the Q band zone, resulting in a shift from ≈ 541 nm to ≈ 533 nm, and a noticeable absorbance increase and shape change of the most intense band (Figure 4). Both spectral changes (especially in the Q band zone) are surprisingly consistent with previously

reported spectra of other iron-nitroxyl heme complexes in organic media.[22] **3** also eventually oxidizes to **1**, with a half-life of about 10 minutes, although further analysis and reactivity studies will be pursued in a different work.

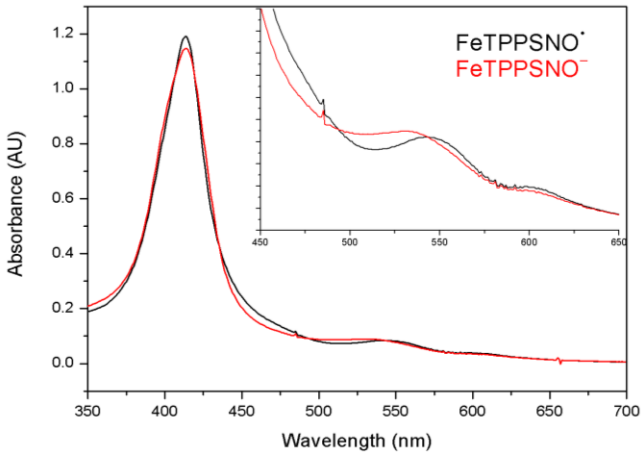

Figure 4. UV-Vis Spectral changes observed upon reduction of Fe^{II}TPPSNO• at pH = 12.

In order to confirm the identity of the product, NaOH was added to the cuvette once **2** was formed at pH 6, rapidly rising the pH to 12. The spectrum assigned to **3** was instantly observed as a result (Figure S5, Scheme 3A). Correspondingly, the formation of **2** was observed after lowering the pH from 11 to 6 by adding HBF_4 to a cuvette containing initially **3**. (Figure S5, Scheme 3B) Therefore, the UV-vis spectra could be correctly assigned to both Fe^{II}TPPSHNO and Fe^{II}TPPSNO⁻ species. Spectroscopic data for the Soret and the main Q band for compounds **1-3** can be found in Table 1.

Scheme 3. Fe^{II}TPPSHNO and Fe^{II}TPPSNO− formation and deprotonation/protonation reactions.

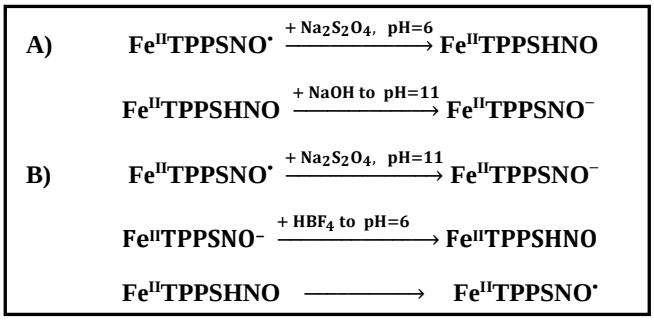

Table 1. UV-Vis spectroscopic data for Fe^{II}TPPS-NO compounds.

	λ_{max}/nm (ε/$M^{-1}cm^{-1}$)
Fe^{II}TPPSNO• (**1**)	414 (155000)[a], 543 (11300)[a]
Fe^{II}TPPSHNO pH = 6 (**2**)	418 (217000), 541(12600)
Fe^{II}TPPSNO⁻ pH = 12 (**3**)	413 (146000), 533 (12000)

Table 1. UV-vis spectroscopic data for Fe^{II}TPPS nitrosyl and nitroxyl compounds in aqueous buffer solutions. a: Reference 35.

pKa estimation

In order to estimate the pKa value associated to the Fe^{II}TPPSHNO/Fe^{II}TPPSNO⁻ acid/base pair, experiments were carried out in different buffers ranging from pH 5 to 11. On one hand, chemical reductions of **1** with dithionite were followed by UV-vis spectrophotometry in order to stablish at which point the obtained spectra for the {FeNO}[8] adduct changed. UV-Vis spectral changes were monitored at pH range 5-11 (See Figures S6-S12 in Supporting Information). Spectral evidence for the protonated adduct could be observed at pH = 9, but not at pH = 10. On the other hand, evidence for the deprotonated species, was observed at pH = 10, but not below. This suggests that the pKa value for **2** would be between 9 and 10, a value similar to the one reported for a ruthenium nitroxyl complex [36]

On the other hand, cyclic voltammetry experiments were made to study the pH dependence of the reduction potential involved. An Fe^{II}TPPSNO• to Fe^{II}TPPSHNO reduction process would depend on H^+ concentration, whereas an Fe^{II}TPPSNO•/ Fe^{II}TPPSNO⁻ reduction would not. At pH = 6, an irreversible strong reduction peak assignable to the Fe^{II}TPPSNO•/Fe^{II}TPPSHNO couple was observed at -0.665 V vs. Ag/AgCl, in concordance with previous reports.[37] At pH = 11.3, the irreversible reductive current wave had effectively shifted to more negative potentials, reaching the peak at -0.885 V for the Fe^{II}TPPSNO•/Fe^{II}TPPSNO⁻ couple vs. Ag/AgCl. The complete set of reductive waves at different pHs values are shown in Figure 5.

The peak current potential shifts as a function of pH can also be used to estimate the pKa of **2**. Nernst's equation for the Fe^{II}TPPSNO•/Fe^{II}TPPSHNO redox process involving one electron and one proton at 298K, predicts a shift of -59 mV per pH unit until the pKa is reached. This behavior is clearly observed for pHs 6-9 (Figure 6), with an experimental slope of -52 mV (see Figure S13). The curve shown in Figure 6 represents the expected behavior for the reduction potential assuming an acidity constant, K_a, of $2x10^{-10}$, estimating a pKa of about 9.7 for Fe^{II}TPPSHNO, consistent with observations done in UV-vis experiments previously described. It is important to note that irreversible current peaks were used for this estimation. Previous reports show the use of irreversible peak data to obtain related useful thermochemical data.[38] Therefore, we believe the method can be used as a

semiquantitative estimation alongside the UV-measurements.

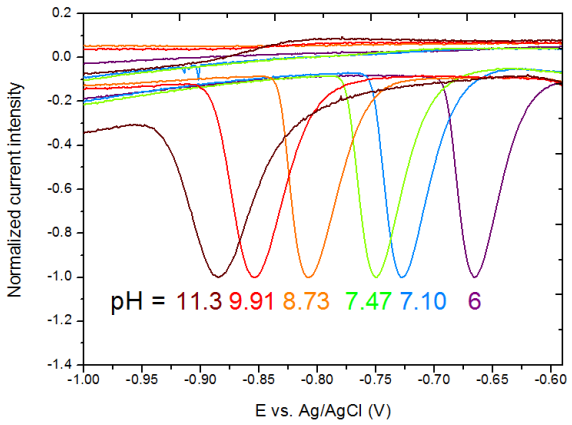

Figure 5. Reductive electrochemical wave assigned to the {FeTPPSNO}^{7}/{FeTPPSNO}^{8} couple for pHs 6 – 11. Current intensities are normalized.

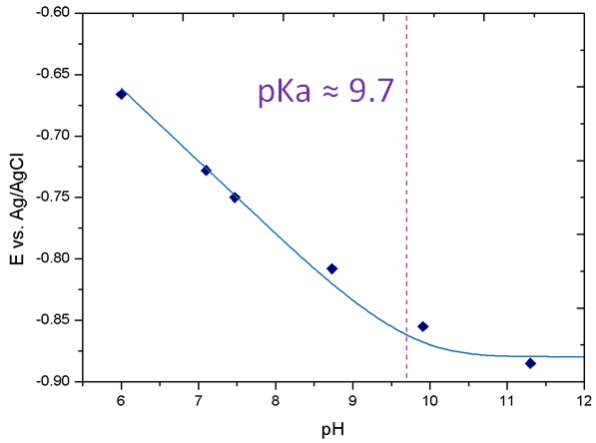

Figure 6. Reduction potential for {FeTPPSNO}^{7}/{FeTPPSNO}^{8} as a function of pH. Experimental measurements are shown along with expected fitting for pKa = 9.7. Linear fitting for pH 6-9 and extra information about CV experiments are shown in Supplementary Information.

This pKa value of 9.7 for Fe^{II}TPPSHNO resulted much higher than the previously estimated value of 2.6 from electrochemical experiments using Fe^{II}TPPSNO$^{\bullet}$ generated *in situ* from the ferric porphyrin and excess nitrite.[37] It is also considerably lower than the revised value reported for free HNO (11.7)[39], and two units higher than the pKa proposed for the pentacyano complex, $[Fe(CN)_5(HNO)]^{3-}$ (7.7),[26] in aqueous solution. The presented result, however, is in excellent agreement with the value reported for $[Ru(Me_3[9]aneN_3)(bpy)(NO)]^{+1}$, which displayed a pKa of 9.8 [36], and falls within the 8-10 range for the pKa value for Fe^{II}OEP(HNO) estimated by FTIR spectroscopy.[19]

Reoxidation reaction studies: kinetic measurements

Many hypotheses were considered in order to elucidate why spontaneous reoxidation took place for the protonated **2** adduct. Although complete absence of oxygen traces cannot be guaranteed, the reproducibility in the experiments led us to think that something other than adventitious oxygen was driving this process. Besides, the expectedly more air-sensitive deprotonated adduct, **3**, seemed to last longer in the cuvette.

Another hypothesis contemplated the possibility of excess NO (g) present in the cuvette displacing HNO as a ligand. However, this was disregarded when the same results were observed using isolated **1** as the starting material, NO gas not being present in excess anymore. In other experiments, when excess NO (g) was purposely added to **2** formed *in situ*, **1** was formed instantly, indicating a probable ligand exchange reaction.

A third hypothesis included the bimolecular decomposition reaction previously proposed in literature[22]:

$$2\ Fe^{II}TPPSHNO\ (aq) \rightarrow 2\ Fe^{II}TPPSNO^{\bullet}(aq) + H_2(g) \quad (1)$$

In order to test this last case, the system was properly optimized in order to make robust kinetic measurements, since processes of this kind have been previously proposed in literature in organic media, but not tested directly.[22]

Kinetic measurements of the reoxidation reaction were carried out under different conditions, being the most robust those carried out in 2 mM phosphate buffer at pH = 6, using a 2 mm pathlength quartz cuvette at room temperature. Integral method plots showed that the decomposition reaction followed a first order decay and not a second order decay, as expected for the reaction shown in Eq. 1. (See Figure S14). Further fitting gave an exponential decay as shown in Figure 7.

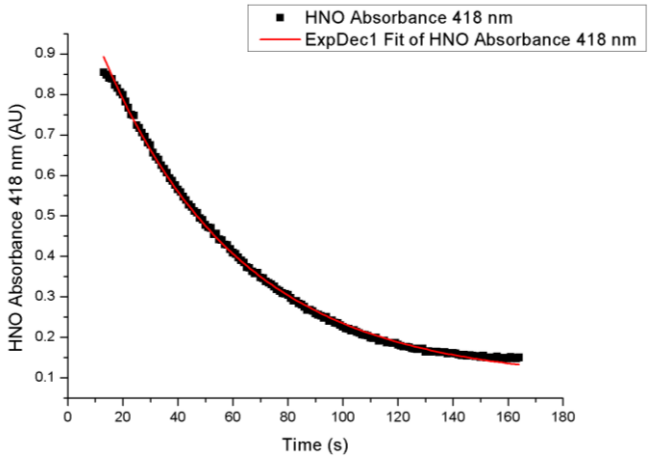

Figure 7. Fe^{II}TPPSHNO absorbance time traces at 418 nm for one selected experiment, which fit a monoexponential decay. See SI (Figures S15-S22) for more representative fittings under different conditions.

The observed first order kinetic constant under these conditions is k= 0.017 ± 0.003 s^{-1}, which accounts for a half-life time of approximately 41 s, considerably longer that the previously reported lifetime of 2 s.[35] It is important to point out that in those conditions, **2** was generated in the presence of glucose and benzophenone radicals, which possibly interfered in the stability of the HNO moiety resulting in a shorter lifespan. These results ruled the bimolecular

reaction hypothesis out and left us with two possibilities: either the reoxidation was an intrinsic first order decomposition of **2**, or a *pseudo* first order decay, involving water or buffer species available in the system. However, no significant differences were observed when buffer was excluded and pure water was used as a solvent, or different buffer compositions were used (Table 2).

The rate constant was determined under different experimental conditions in order to find possible reoxidation paths (Table 2). The pHs = 5, 6 and 7 gave out virtually the same reoxidation rate. Surprisingly, the only significantly different rate, greater by an order of magnitude, was observed when using Cr^{II}EDTA as a reducing agent (Table 2, row 4). This led us to think that either the metallic traces in Cr^{II}EDTA or the chromium complex itself catalyzed the oxidation reaction, or that, inversely, when dithionite was used as a reducing agent, the reaction proceeded more slowly. This could be a consequence of dithionite byproducts, such as sulfite, coordinating to **2** in the sixth position. However, dithionite experiments in presence of metallic traces (Cr^{3+}, Fe^{3+}) did not show significant differences; the same was observed when excess sulfite was added to the cuvette before reduction.

The reaction was also carried out in presence of excess imidazole at pH 7 to determine if coordination of an axial sixth ligand would relatively stabilize **2**. The obtained kinetic constant was fairly smaller than in its absence (Table 2, row 7), suggesting a somewhat stabilizing effect of the axial ligand.

Finally, when the experiment was carried out in phosphate buffer dissolved in D_2O, the rate constant was significantly smaller than in H_2O (Table 2, row 3), k_H/k_D being 2.7, which seems to correspond to a primary kinetic isotope effect, in which R-H bond breakage is involved in the transition state. Therefore, the H-NO bond breaking is involved in the limiting step of the reoxidation reaction. However, it could also implicate that water attacks **2** to give **1** and byproducts through a *pseudo* first order mechanism.

Table 2. Kinetic constants for Fe^{II}TPPSHNO under different contidions

Row n°	Experimental conditions	k (s^{-1})	N
1	Phosphate buffer pH 6, 2 mM Reducing agent: $Na_2S_2O_4$	0.017 ± 0.003	13
2	Phosphate buffer pH 6 2 mM Reducing agent: $Na_2S_2O_4$ Sulphite excess	0.014 ± 0.003	3
3	Phosphate buffer pH 6, 2 mM in D_2O Reducing agent: $Na_2S_2O_4$	0.0064 ± 0.0003	3
4	Phosphate buffer pH 6, 2 mM Reducing agent: Cr^{II}(EDTA)	0.17 ± 0.06	10
5	Citrate buffer pH 5, 2 mM Reducing agent: $Na_2S_2O_4$	0.019 ± 0.009	3
6	Phosphate buffer pH 7, 2 mM Reducing agent: $Na_2S_2O_4$	0.017 ± 0.002	4
7	Phosphate buffer pH 7, 2 mM Reducing agent: $Na_2S_2O_4$ Imidazole excess	0.010 ± 0.002	3
8	Deionized water Reducing agent: $Na_2S_2O_4$	0.025 ± 0.007	7

Table 2. Kinetic constants for the spontaneous reoxidation of Fe^{II}TPPSHNO to Fe^{II}TPPSNO$^{\bullet}$ measured under different experimental conditions, along their standard deviation. N is the number of experiments considered for each experimental condition.

Given these results, reoxidation of **2** to **1** by loss of an H atom through homolytic rupture of the N-H bond (Scheme 4). The significantly different value obtained for the reduction with Cr^{II}EDTA could be explained by a possible hydrogen atom abstraction activity carried out by this compound or its byproducts.

Scheme 4. Proposed homolytic decomposition of Fe^{II}TPPSHNO

$$Fe^{II}TPPSHNO \rightarrow Fe^{II}TPPSNO^{\bullet} + H^{\bullet}$$

In order to indirectly test this hypothesis, UV reduction experiments were carried out in the presence of the free-radical TEMPO, which has the ability to abstract H$^{\bullet}$ radicals and form TEMPOH. Previous studies[40] show that the H-N bond energy in HNO (49.9 kcal/mol) is substantially smaller than the average H-N bond (90 kcal/mol), making it relatively easy to break. The reaction of free HNO with TEMPOL has already been studied, resulting in a hydrogen atom abstraction to give NO$^{\cdot}$ and TEMPOL-H.[41] With this in mind, 2 eq. of TEMPO were added to a cuvette containing freshly formed **2** at pH = 6 (by dithionite reduction of **1**). Complete and instantaneous formation of **1** was observed instead of the progressive oxidation witnessed in analogous experiments in the absence of TEMPO. This qualitative experiment shows that the H$^{\bullet}$ in the Fe-HNO moiety is readily abstracted, in concordance with the proposed decomposition pathway of Scheme 4.

This decomposition pathway would also explain why the deprotonated adduct has a longer lifetime, since it is not susceptible to homolytic bond-breaking.

DFT calculations – formation of phlorin intermediate

DFT calculations were performed using the FeTPP model in order to gain more insight into the reoxidation mechanism of **2**. The structure for Fe^{II}TPPHNO was optimized, and energy scans along the H-N bond of the HNO moiety were performed as bond distance increased. The final structure showed that the hydrogen atom from the HNO moiety had migrated to the most proximate *meso* carbon of the porphyrin ring. This unexpected result led us to optimize the

structures of the final product and the transition state to see if it was a plausible rate-limiting step for a unimolecular reaction. Surprisingly, the final *phlorin* intermediate resulted only 2.4 kcal mol $^{-1}$ higher in energy than the initial Fe^{II}TPPHNO structure, while the calculated activation energy for the interconversion of these tautomers resulted in 19.4 kcal mol $^{-1}$ (Figure 8). Intramolecular proton-coupled electron transfers of this kind have been recently reported for other porphyrins, where the bent *phlorin* intermediate was theoretically proposed and detected.[42–45]

The energy associated with reaction (2) was also calculated, in order to dismiss a *pseudo* first order mechanism involving water. As expected for the formation of a reactive OH$^{\bullet}$ radical, the reaction resulted thermodynamically uphill by 93.1 kcal mol $^{-1}$.

$$Fe^{II}TPPSHNO\ (aq) + H_2O \rightarrow \rightarrow Fe^{II}TPPSNO^{\bullet}(aq) + H_2(g) + OH^{\bullet}(aq) \quad (2)$$

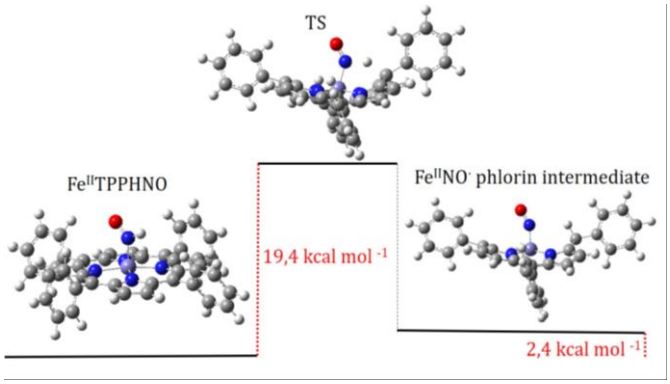

Figure 8. Optimized structures and calculated energy differences for Fe^{II}TPPHNO, the final phlorin intermediate and transition state.

The performed calculations support a first order decomposition mechanism in agreement with the experimental measurements, in which the rate-determining step consists in the formation of the unstable *phlorin* intermediate. This species, which was not detected via UV-vis measurements, would rapidly react re-donating the H$^{\bullet}$ entity to give unspecified products and the $Fe^{II}NO^{\bullet}$ moiety.

For the first time, the reoxidation kinetics for a bound HNO moiety could be measured, resulting in a first order unimolecular reaction which in turn could be reasonably explained by pertinent calculations. We note that this mechanism does not agree with the previously suggested bimolecular decomposition which supported the greater stability of the HNO complex of a sterically hindered *picket fence* porphyrin.[22] On one hand, we are aware that aqueous and organic media chemistry are different and therefore decomposition mechanisms might not be the same. On the other hand, the greater stability of the hindered porphyrin could also be due to the fact that the bulky substituents prevent the structure from bending and transferring the H$^{\bullet}$ atom to the *meso* carbon in an effective manner. Additional investigations should be carried out to further study these systems.

Conclusions

A water-soluble iron nitrosyl porphyrin complex, Fe^{II}TPPSNO$^{\bullet}$ was obtained through two different routes and successfully isolated for the first time as a solid. This compound turned out to be stable for many months if stored under argon. This product was characterized by FT-IR, cyclic voltammetry, elemental analysis and UV-visible techniques.

Reduction of Fe^{II}TPPSNO$^{\bullet}$ at different pHs showed UV-Vis spectroscopic evidence for the formation of the first water-soluble ferrous heme nitroxylcomplexes Fe^{II}TPPSHNO and Fe^{II}TPPSNO^{-}. This information, along with data from electrochemical measurements allowed us to estimate the pKa value for the Fe^{II}TPPSHNO/Fe^{II}TPPSNO^{-} equilibrium to be around 9.7.

Both complexes eventually reoxidize to the initial nitrosyl species, with an estimated half-time life of 10 min for Fe^{II}TPPSNO^{-} and less than a minute for Fe^{II}TPPSHNO.

Plausible causes for Fe^{II}TPPSHNO instability were evaluated, and most of them were ruled out. The reoxidation reaction is an order 1 decay in pH = 6 phosphate buffer, with an estimated k = 0.017 s^{-1} ($t_{1/2}$ = 41 s, considerably greater than the one previously reported)[14]. Our results strongly indicate that the Fe^{II}TPPSHNO moiety undergoes an homolytic bond break, resulting in the observed Fe^{II}TPPSNO$^{\bullet}$ and H$^{\bullet}$ which due to its high reactivity further reacts with solvent and/or other species (such us buffer and the byproducts of the reducing agents) This hypothesis is supported by experiments carried out in the presence of H$^{\bullet}$ withdrawing compounds (TEMPO) and DFT calculations that predict homolytic H-NO bond cleavage and intramolecular addition to the porphyrin *meso* carbon to give a *phlorin* intermediate. Despite this apparently rapid reoxidation, the protonated nitroxyl species turned out to be substantially more stable than its organic-media analogues previously reported. This observation agrees with the proposed hypothesis that hydrogen bonds with water help to stabilize the Fe-HNO moiety.

Further experiments will be carried out to continue investigating these new important biomimetic complexes, in order to evaluate their reactivity with biologically relevant substrates. The decomposition pathway of Fe^{II}TPPSNO^{-} must also be explored and understood, hoping to increase its stability and carry our more rigorous characterization and reactivity studies.

In addition, other water-soluble platforms will be studied. In particular, experiments with cationic porphyrins like meso-tetra(N-methylpyridyl)porphyrin (TMPyP) could provide valuable insight on the influence of the charge of the ligand on the stability of nitroxyl compounds.

ASSOCIATED CONTENT

Supporting Information. Complementary IR, NMR and UV spectra, cyclic voltammetry considerations, additional kinetic fittings and useful structures are shown in Supporting information. This material is available free of charge via the Internet at http://pubs.acs.org.

AUTHOR INFORMATION

Corresponding Author

* Juan Pellegrino: pellegrino@qi.fcen.uba.ar
* Fabio Doctorovich: doctorovich@qi.fcen.uba.ar

Funding Sources

We thank CONICET, UBA (grant UBACYT 2018) and ANPCYT (PICT-2017-1930) for the necessary funding for this work.

ACKNOWLEDGMENT

We thank Dr. Gabriel Gordillo for the electrochemical measurements and Federico Davia for the provided assistance. F.D. and J.P. are CONICET members, and A. M. M. is a CONICET doctoral fellow.

ABBREVIATIONS

TPPS = Meso-tetra(4-sulfonatophenyl)porphine

REFERENCES

(1) Culotta, E.; Koshland, D. NO News Is Good News. *Science* **1992**, *258* (5090), 1862. https://doi.org/10.1126/science.1361684.

(2) Thomas, D. D.; Ridnour, L. A.; Isenberg, J. S.; Flores-Santana, W.; Switzer, C. H.; Donzelli, S.; Hussain, P.; Vecoli, C.; Paolocci, N.; Ambs, S.; et al. The Chemical Biology of Nitric Oxide: Implications in Cellular Signaling. *Free Radical Biology and Medicine* **2008**, *45* (1), 18–31. https://doi.org/10.1016/j.freeradbiomed.2008.03.020.

(3) Suarez, S. A.; Muñoz, M.; Alvarez, L.; Venâncio, M. F.; Rocha, W. R.; Bikiel, D. E.; Marti, M. A.; Doctorovich, F. HNO Is Produced by the Reaction of NO with Thiols. *J. Am. Chem. Soc.* **2017**, *139* (41), 14483–14487. https://doi.org/10.1021/jacs.7b06968.

(4) Suarez, S. A.; Neuman, N. I.; Muñoz, M.; Álvarez, L.; Bikiel, D. E.; Brondino, C. D.; Ivanović-Burmazović, I.; Miljkovic, J. Lj.; Filipovic, M. R.; Martí, M. A.; et al. Nitric Oxide Is Reduced to HNO by Proton-Coupled Nucleophilic Attack by Ascorbate, Tyrosine, and Other Alcohols. A New Route to HNO in Biological Media? *J. Am. Chem. Soc.* **2015**, *137* (14), 4720–4727. https://doi.org/10.1021/ja512343w.

(5) Marti, M. A.; Álvarez, L.; Suarez, S. A.; Doctorovich, F. 18 - Is Azanone Endogenously Produced in Mammals? In *The Chemistry and Biology of Nitroxyl (HNO)*; Doctorovich, F., Farmer, P. J., Marti, M. A., Eds.; Elsevier: Boston, 2017; pp 337–351. https://doi.org/10.1016/B978-0-12-800934-5.00018-9.

(6) Ma, X. L.; Gao, F.; Liu, G.-L.; Lopez, B. L.; Christopher, T. A.; Fukuto, J. M.; Wink, D. A.; Feelisch, M. Opposite Effects of Nitric Oxide and Nitroxyl on Postischemic Myocardial Injury. *PNAS* **1999**, *96* (25), 14617–14622. https://doi.org/10.1073/pnas.96.25.14617.

(7) Paolocci, N.; Keceli, G.; Wink, D. A.; Kass, D. A. From Heaven to Heart: Nitroxyl (HNO) in the Cardiovascular System and Beyond. *The Chemistry and Biology of Nitroxyl (HNO)* **2016**, 353–387. https://doi.org/10.1016/B978-0-12-800934-5.00019-0.

(8) Flores-Santana, W.; Salmon, D. J.; Donzelli, S.; Switzer, C. H.; Basudhar, D.; Ridnour, L.; Cheng, R.; Glynn, S. A.; Paolocci, N.; Fukuto, J. M.; et al. The Specificity of Nitroxyl Chemistry Is Unique Among Nitrogen Oxides in Biological Systems. *Antioxidants & Redox Signaling* **2011**, *14* (9), 1659–1674. https://doi.org/10.1089/ars.2010.3841.

(9) Vásquez, M. A. M.; Pellegrino, J.; Álvarez, L.; Neuman, N. I.; Doctorovich, F.; Martí, M. A. 9 - Interactions of HNO With Metallated Porphyrins, Corroles, and Corrines. In *The Chemistry and Biology of Nitroxyl (HNO)*; Doctorovich, F., Farmer, P. J., Marti, M. A., Eds.; Elsevier: Boston, 2017; pp 193–205. https://doi.org/10.1016/B978-0-12-800934-5.00009-8.

(10) Averill, B. A. Dissimilatory Nitrite and Nitric Oxide Reductases. *Chem. Rev.* **1996**, *96* (7), 2951–2964. https://doi.org/10.1021/cr950056p.

(11) Zumft, W. G. The Biological Role of Nitric Oxide in Bacteria. *Arch. Microbiol.* **1993**, *160* (4), 253–264. https://doi.org/10.1007/BF00292074.

(12) Shiro, Y.; Fujii, M.; Isogai, Y.; Adachi, S.; Iizuka, T.; Obayashi, E.; Makino, R.; Nakahara, K.; Shoun, H. Iron-Ligand Structure and Iron Redox Property of Nitric Oxide Reductase Cytochrome P450nor from Fusarium Oxysporum: Relevance to Its NO Reduction Activity. *Biochemistry* **1995**, *34* (28), 9052–9058. https://doi.org/10.1021/bi00028a014.

(13) Enemark, J. H.; Feltham, R. D. Principles of Structure, Bonding, and Reactivity for Metal Nitrosyl Complexes. *Coordination Chemistry Reviews* **1974**, *13* (4), 339–406. https://doi.org/10.1016/S0010-8545(00)80259-3.

(14) Speelman, A. L.; Lehnert, N. Heme versus Non-Heme Iron-Nitroxyl {FeN(H)O}8 Complexes: Electronic Structure and Biologically Relevant Reactivity. *Acc. Chem. Res.* **2014**, *47* (4), 1106–1116. https://doi.org/10.1021/ar400256u.

(15) Lancon, D.; Kadish, K. M. Electrochemical and Spectral Characterization of Iron Mono- and Dinitrosyl Porphyrins. *J. Am. Chem. Soc.* **1983**, *105* (17), 5610–5617. https://doi.org/10.1021/ja00355a014.

(16) Olson, L. W.; Schaeper, D.; Lancon, D.; Kadish, K. M. Characterization of Several Novel Iron Nitrosyl Porphyrins. *J. Am. Chem. Soc.* **1982**, *104* (7), 2042–2044. https://doi.org/10.1021/ja00371a051.

(17) Choi, I. Kyu.; Liu, Yanming.; Feng, DiWei.; Paeng, K. Jung.; Ryan, M. D. Electrochemical and Spectroscopic Studies of Iron Porphyrin Nitrosyls and Their Reduction Products. *Inorg. Chem.* **1991**, *30* (8), 1832–1839. https://doi.org/10.1021/ic00008a028.

(18) Wei, Z.; Ryan, M. D. Infrared Spectroelectrochemical Reduction of Iron Porphyrin Complexes. *Inorg. Chem.* **2010**, *49* (15), 6948–6954. https://doi.org/10.1021/ic100614h.

(19) Rahman, Md. H.; Ryan, M. D. Redox and Spectroscopic Properties of Iron Porphyrin Nitroxyl in the Presence of Weak Acids. *Inorg. Chem.* **2017**, *56* (6), 3302–3309. https://doi.org/10.1021/acs.inorgchem.6b02665.

(20) Abucayon, E. G.; Khade, R. L.; Powell, D. R.; Zhang, Y.; Richter-Addo, G. B. Hydride Attack on a Coordinated Ferric Nitrosyl: Experimental and DFT Evidence for the Formation of a Heme Model–HNO Derivative. *J. Am. Chem. Soc.* **2016**, *138* (1), 104–107. https://doi.org/10.1021/jacs.5b12008.

(21) Pellegrino, J.; Bari, S. E.; Bikiel, D. E.; Doctorovich, F. Successful Stabilization of the Elusive Species {FeNO} ^{8} in a Heme Model. *J. Am. Chem. Soc.* **2010**, *132* (3), 989–995. https://doi.org/10.1021/ja905062w.

(22) Goodrich, L. E.; Roy, S.; Alp, E. E.; Zhao, J.; Hu, M. Y.; Lehnert, N. Electronic Structure and Biologically Relevant Reactivity of Low-Spin {FeNO}8 Porphyrin Model Complexes: New Insight from a Bis-Picket Fence Porphyrin. *Inorg. Chem.* **2013**, *52* (13), 7766–7780. https://doi.org/10.1021/ic400977h.

(23) Lin, R.; Farmer, P. J. The HNO Adduct of Myoglobin: Synthesis and Characterization. *J. Am. Chem. Soc.* **2000**, *122* (10), 2393–2394. https://doi.org/10.1021/ja994079n.

(24) Kumar, M. R.; Pervitsky, D.; Chen, L.; Poulos, T.; Kundu, S.; Hargrove, M. S.; Rivera, E. J.; Diaz, A.; Colón, J. L.; Farmer, P. J. Nitrosyl Hydride (HNO) as an O2 Analogue: Long-Lived HNO Adducts of Ferrous Globins. *Biochemistry*

2009, *48* (22), 5018–5025. https://doi.org/10.1021/bi900122r.

(25) Immoos, C. E.; Sulc, F.; Farmer, P. J.; Czarnecki, K.; Bocian, D. F.; Levina, A.; Aitken, J. B.; Armstrong, R. S.; Lay, P. A. Bonding in HNO-Myoglobin as Characterized by X-Ray Absorption and Resonance Raman Spectroscopies. *J. Am. Chem. Soc.* **2005**, *127* (3), 814–815. https://doi.org/10.1021/ja0433727.

(26) Montenegro, A. C.; Amorebieta, V. T.; Slep, L. D.; Martín, D. F.; Roncaroli, F.; Murgida, D. H.; Bari, S. E.; Olabe, J. A. Three Redox States of Nitrosyl: NO+, NO., and NO−/HNO Interconvert Reversibly on the Same Pentacyanoferrate(II) Platform. *Angewandte Chemie International Edition* **2009**, *48* (23), 4213–4216. https://doi.org/10.1002/anie.200806229.

(27) Fernandez, B. O.; Lorković, I. M.; Ford, P. C. Nitrite Catalyzes Reductive Nitrosylation of the Water-Soluble Ferri-Heme Model FeIII(TPPS) to FeII(TPPS)(NO). *Inorg. Chem.* **2003**, *42* (1), 2–4. https://doi.org/10.1021/ic020519r.

(28) Laverman, L. E.; Ford, P. C. Mechanistic Studies of Nitric Oxide Reactions with Water Soluble Iron(II), Cobalt(II), and Iron(III) Porphyrin Complexes in Aqueous Solutions: Implications for Biological Activity. *J. Am. Chem. Soc.* **2001**, *123* (47), 11614–11622. https://doi.org/10.1021/ja0113910.

(29) McKenna, C. E.; Gutheil, W. G.; Song, W. A Method for Preparing Analytically Pure Sodium Dithionite. Dithionite Quality and Observed Nitrogenase-Specific Activities. *Biochimica et Biophysica Acta (BBA) - General Subjects* **1991**, *1075* (1), 109–117. https://doi.org/10.1016/0304-4165(91)90082-R.

(30) Mason, J.; Larkworthy, L. F.; Moore, E. A. Nitrogen NMR Spectroscopy of Metal Nitrosyls and Related Compounds. *Chem. Rev.* **2002**, *102* (4), 913–934. https://doi.org/10.1021/cr000075l.

(31) Fleischer, E. B.; Palmer, J. M.; Srivastava, T. S.; Chatterjee, A. Thermodyamic and Kinetic Properties of an Iron-Porphyrin System. *J. Am. Chem. Soc.* **1971**, *93* (13), 3162–3167. https://doi.org/10.1021/ja00742a012.

(32) Bari, S. E.; Martí, M. A.; Amorebieta, V. T.; Estrin, D. A.; Doctorovich, F. Fast Nitroxyl Trapping by Ferric Porphyrins. *J. Am. Chem. Soc.* **2003**, *125* (50), 15272–15273. https://doi.org/10.1021/ja036370f.

(33) Porcheddu, A.; Luca, L. D.; Giacomelli, G. A Straightforward Route to Piloty's Acid Derivatives: A Class of Potential Nitroxyl-Generating Prodrugs. *Synlett* **2009**, *2009* (13), 2149–2153. https://doi.org/10.1055/s-0029-1217565.

(34) Aizawa, K.; Nakagawa, H.; Matsuo, K.; Kawai, K.; Ieda, N.; Suzuki, T.; Miyata, N. Piloty's Acid Derivative with Improved Nitroxyl-Releasing Characteristics. *Bioorganic & Medicinal Chemistry Letters* **2013**, *23* (8), 2340–2343. https://doi.org/10.1016/j.bmcl.2013.02.062.

(35) Seki, H.; Hoshino, M.; Kounose, S. Reduction of a Water-Soluble Iron(III) Porphyrin and an Iron(II) Nitrosyl Porphyrin by Benzophenone Ketyl Radical. *J. Chem. Soc., Faraday Trans.* **1996**, *92* (14), 2579–2583. https://doi.org/10.1039/FT9969202579.

(36) Codesido, N. O.; Weyhermüller, T.; Olabe, J. A.; Slep, L. D. Nitrosyl-Centered Redox and Acid–Base Interconversions in [Ru(Me3[9]AneN3)(Bpy)(NO)]3,2,1+. The PKa of HNO for Its Nitroxyl Derivative in Aqueous Solution. *Inorg. Chem.* **2014**, *53* (2), 981–997. https://doi.org/10.1021/ic402448p.

(37) Barley, M. H.; Meyer, T. J. Electrocatalytic Reduction of Nitrite to Ammonia Based on a Water-Soluble Iron Porphyrin. *J. Am. Chem. Soc.* **1986**, *108* (19), 5876–5885. https://doi.org/10.1021/ja00279a036.

(38) Bordwell, F. G.; Cheng, J. Pei.; Harrelson, J. A. Homolytic Bond Dissociation Energies in Solution from Equilibrium Acidity and Electrochemical Data. *J. Am. Chem. Soc.* **1988**, *110* (4), 1229–1231. https://doi.org/10.1021/ja00212a035.

(39) Shafirovich, V.; Lymar, S. V. Nitroxyl and Its Anion in Aqueous Solutions: Spin States, Protic Equilibria, and Reactivities toward Oxygen and Nitric Oxide. *Proc Natl Acad Sci USA* **2002**, *99* (11), 7340. https://doi.org/10.1073/pnas.112202099.

(40) Dixon, R. N. The Heats of Formation of HNO and of DNO. *J. Chem. Phys.* **1996**, *104* (17), 6905–6906. https://doi.org/10.1063/1.471714.

(41) Miranda, K. M.; Paolocci, N.; Katori, T.; Thomas, D. D.; Ford, E.; Bartberger, M. D.; Espey, M. G.; Kass, D. A.; Feelisch, M.; Fukuto, J. M.; et al. A Biochemical Rationale for the Discrete Behavior of Nitroxyl and Nitric Oxide in the Cardiovascular System. *Proc Natl Acad Sci USA* **2003**, *100* (16), 9196. https://doi.org/10.1073/pnas.1430507100.

(42) Solis, B. H.; Maher, A. G.; Honda, T.; Powers, D. C.; Nocera, D. G.; Hammes-Schiffer, S. Theoretical Analysis of Cobalt Hangman Porphyrins: Ligand Dearomatization and Mechanistic Implications for Hydrogen Evolution. *ACS Catal.* **2014**, *4* (12), 4516–4526. https://doi.org/10.1021/cs501454y.

(43) Fang, Y.; Gorbunova, Y. G.; Chen, P.; Jiang, X.; Manowong, M.; Sinelshchikova, A. A.; Enakieva, Y. Yu.; Martynov, A. G.; Tsivadze, A. Yu.; Bessmertnykh-Lemeune, A.; et al. Electrochemical and Spectroelectrochemical Studies of Diphosphorylated Metalloporphyrins. Generation of a Phlorin Anion Product. *Inorg. Chem.* **2015**, *54* (7), 3501–3512. https://doi.org/10.1021/acs.inorgchem.5b00067.

(44) Kadish, K. M.; Sazou, D.; Liu, Y. M.; Saoiabi, A.; Ferhat, M.; Guilard, R. Electrochemical and Spectroelectrochemical Studies of Nickel(II) Porphyrins in Dimethylformamide. *Inorg. Chem.* **1988**, *27* (7), 1198–1204. https://doi.org/10.1021/ic00280a021.

(45) Solis, B. H.; Maher, A. G.; Dogutan, D. K.; Nocera, D. G.; Hammes-Schiffer, S. Nickel Phlorin Intermediate Formed by Proton-Coupled Electron Transfer in Hydrogen Evolution Mechanism. *PNAS* **2016**, *113* (3), 485–492. https://doi.org/10.1073/pnas.1521834112.